Journal of Power Sources 195 (2010) 271–279

Contents lists available at ScienceDirect

Journal of Power Sources

journal homepage: www.elsevier.com/locate/jpowsour

Stability and coking of direct-methane solid oxide fuel cells: Effect of CO_2 and air additions

Manoj Pillai[a], Yuanbo Lin[a], Huayang Zhu[b], Robert J. Kee[b], Scott A. Barnett[a,*]

[a] Materials Science, Northwestern University, Evanston, IL 60208, USA
[b] Engineering Division, Colorado School of Mines, Golden, CO 80401, USA

ARTICLE INFO

Article history:
Received 26 March 2009
Received in revised form 16 May 2009
Accepted 18 May 2009
Available online 23 May 2009

Keywords:
SOFC
Methane
Stability
Barrier layer

ABSTRACT

This paper concerns the stability of anode-supported solid oxide fuel cells (SOFCs), operated with fuel mixtures of methane–CO_2 and methane–air. Stability, which was evaluated in terms of voltage decrease at constant current density, was affected by coke deposits. Chemically inert anode barrier layers were shown to enhance stability and to slow catalytic endothermic reforming reactions within the Ni–YSZ anode that otherwise caused deleterious temperature variations and cell cracking. Increasing the amount of CO_2 added to CH_4 fuel led to a wider stable operating range, yet had relatively little effect on SOFC performance. Button cells operated at 800 °C with fuel streams of 75% CH_4 and 25% CO_2 achieved maximum power densities above 1 W/cm^2. Adding air to methane also increased stability. In the case of air addition, SOFC temperature increased as a consequence of exothermic partial-oxidation reforming chemistry. Models were developed to predict temperature and gas-composition profiles within the button cells. The simulation results were used to assist interpretation of the experimental observations.

1. Introduction

There are potentially great benefits associated with the development of solid oxide fuel cells (SOFCs) that can be fueled directly with natural gas. Benefits include the elimination or simplification of upstream fuel-reforming components, and thus reduced system cost [1,2]. However, for such technology to be considered seriously, scientific issues associated with anode coking (especially for Ni-based anodes) must be understood. Cell and system designs, together with operating protocols, must be developed to assure long-term stability, and hence technological viability.

It has been shown that methane-fueled, Ni–YSZ anode-supported, SOFCs can operate stably without coking when the cell current density is sufficiently large [3]. The reasons for coke-free operation can be understood (at least qualitatively) in the context of equilibrium graphite formation [4]. Fig. 1 shows the Gibbs C–H–O triangle, with the equilibrium coking and non-coking regions indicated. The point marked CH_4 is well within the coking regime. In an operating fuel cell, fuel is consumed and the oxygen content (in the form of H_2O and CO_2) increases as a result of electrochemical charge transfer. The mixture composition of fuel and reaction products shifts generally toward the non-coking region. Mixing CO_2, air, and H_2O with CH_4 moves the net fuel composition along the three dashed lines in Fig. 1.

The present paper explores two complementary alternatives to expand stable coke-free operating conditions. The first involves explicit addition of oxygen-bearing compounds into the fuel. Experimental results are discussed for CH_4–CO_2 and CH_4–air mixtures. Models are developed and used to interpret the results and to predict the performance of CH_4–H_2O mixtures. CO_2 and H_2O additions could be implemented in practice by recycling the cell exhaust. It is possible to incorporate sufficient oxygen with the fuel to eliminate coking. However, the required oxygen levels are sufficiently high as to degrade fuel-cell performance. Therefore, the cells developed here also include barrier layers [5–7].

The barrier-layer architecture provides advantages compared to conventional internal reforming, where sufficient oxygen-bearing additives are carried in the fuel. The barrier layer is a chemically inert, porous, material (e.g., partially stabilized zirconia, PSZ) that is positioned between the fuel compartment and the anode structural support (e.g., Ni–YSZ). The barrier impedes the flux of fuel onto the catalytically active Ni–YSZ and impedes the flux of CO_2 and H_2O from the anode to the fuel compartment. Consequently the gas-phase composition in contact with Ni (which catalyzes coke formation) can be maintained in the coke-free region (Fig. 1). The barrier serves to reduce the amount of oxygen that must otherwise be carried in the fuel, thus improving cell performance.

In addition to reducing coke formation, barriers are found to offer benefits in moderating temperature variations. Internal hydrocarbon reforming (using either H_2O or CO_2) is a significantly endothermic catalytic process, which tends to cool the Ni–YSZ anode structure. When reforming rates are sufficiently high, the

* Corresponding author. Tel: +1 847 491 2447; fax: +1 847 491 7820.
E-mail address: s-barnett@northwestern.edu (S.A. Barnett).

0378-7753/$ – see front matter © 2009 Elsevier B.V. All rights reserved.
doi:10.1016/j.jpowsour.2009.05.032

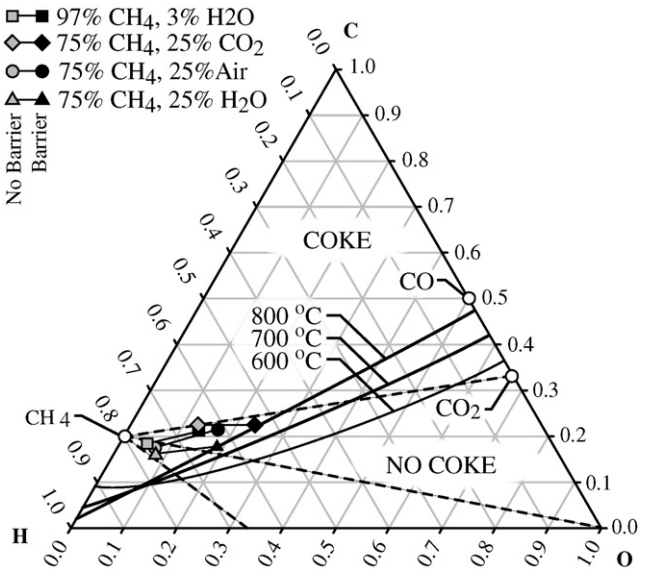

Fig. 1. Gibbs C–H–O triangle showing regions of equilibrium coke formation at three temperatures. Solid carbon (graphite) is stable in equilibrium above the solid lines, which depend upon temperature. Unreacted mixtures of CH_4–CO_2, CH_4–O_2, and CH_4–H_2O fall along the dashed lines. The points indicate modeling results that correspond to experimentally measured cell operating conditions.

cooling induces tensile stresses that can crack the cell. Indeed, structural damage is found to be a significant problem when sufficient CO_2 is mixed with CH_4 to operate below the coking limits. The barrier layer reduces the reforming rates, enabling coke-free operation and improved structural integrity.

Although the present paper concentrates on button cells, the results are useful in the design of stacks and systems. In a typical fuel-cell stack, the region near the cell entrance is usually most susceptible to coking because the hydrocarbon concentrations are high. In downstream regions of the stack, where the fuel has been consumed and diluted by oxygen-bearing reaction products, coking propensity is significantly reduced. Thus, the barrier layer is especially important in the entry regions because it enables the use of hydrocarbon-rich fuels. In other words, the barrier reduces the amount of CO_2, H_2O, or air that must to be mixed with the incoming fuel (including anode recycle) [5–7]. It may also be noted that alternative uses of the fuel cell, including electrochemical partial oxidation to produce syngas and electricity [8–10], benefit from the approaches discussed herein. In such applications the syngas composition (i.e., H_2/CO ratio) can be tuned for further down-stream processing by controlling the levels of H_2O and CO_2 in the fuel stream [11,12].

2. Experimental

The anode-supported SOFCs used in this study consisted of Ni–YSZ anode supports, thin YSZ electrolytes, and LSM–YSZ cathodes. The SOFCs were prepared by standard powder-processing techniques. The supports were prepared by ball milling NiO and YSZ (8 mol% Y_2O_3-stabilized ZrO_2) powder in a ratio of 1:1 by weight, with 10% starch filler and 60 ml ethanol for about 24 h. The powder was used to die press 19-mm (0.75 in.) diameter pellets that were approximately 0.7 mm thick. These were then pre-fired at 1100 ° C for about 4 h, improving mechanical strength and matching shrinkage for further processing and co-firing. A NiO–YSZ anode active layer and a thin dense YSZ electrolyte layer were deposited on the NiO–YSZ supports using a colloidal deposition technique similar to that described previously [13]. The anode–electrolyte bi-layers were fired at 1400 ° C for 4 h, obtaining a dense YSZ electrolyte micro-structure. A bi-layer cathode, comprised of an LSM–YSZ (LSM: $La_{0.8}Sr_{0.2}MnO_3$) layer followed by a pure LSM layer for current collection, completed the SOFC fabrication procedure. The composite layer was fired at 1175 ° C for 1 h, while the pure layer was fired at 1125 ° C for 1 h.

For current collection during SOFC testing, a silver grid was screen printed on top of the LSM layer. There was no current collector on the anode side. The final fuel cells were approximately 15.25 mm (0.6 in.) in diameter, with an anode thickness of approximately 0.6 mm, electrolyte thickness of approximately 10 μm, and cathode thickness of 20–30 μm. Anode porosity was approximately 40% and cathode porosity was approximately 35%. The cathode area, which defined the cell active area, was approximately 0.5 cm^2. Except for initial experiments carried out without barrier layers, the cell tests described below were done with inert porous barrier layers placed against the anodes. Fabrication of barrier layers was described previously [5]. In brief, the barrier layers were PSZ pellets that were approximately 0.4 mm thick with 40% porosity. They had the same diameter as the finished SOFCs.

SOFC electrical testing was carried out in a setup that has been described elsewhere [8]. The cells were initially heated to 700–750 ° C in humidified hydrogen in order to reduce the anode NiO to Ni, maintained for approximately 12 h to eliminate initial transients, and then baseline electrical testing was carried out in humidified hydrogen. Stability tests were then performed at 700, 750, and 800 ° C with different fuel mixtures. A 30 sccm (standard cubic centimeter per minute) flow rate of CH_4 was used, unless otherwise specified, for pure CH_4 and fuel mixtures. For CH_4–CO_2 mixtures, the CO_2 flow rates were between 10 and 16 sccm. For CH_4–air mixtures, the air flow rate was 10 sccm. Cell voltage was measured versus time at fixed current density J for approximately 8 h. The constant-current test was then repeated at lower J values until the cell voltage became unstable; after unstable operation for a few hours, coking was usually observed on the anodes [3,5]. A voltage decrease of less than 5 mV over 8 h was considered to be stable performance. Under such conditions, no carbon was detected by SEM-EDS on the anodes [3,5]. Finally, experiments were carried out in which the constant current was interrupted (i.e., decreased to $J = 0$) for different periods of time before returning to the initial J value.

Steam-methane fuel mixtures are certainly of technological interest. However, this study did not include such experiments. Experimentally, it is easier to accurately control CO_2 partial pressure than H_2O partial pressure. There is reason to believe that CH_4–CO_2 mixtures will behave similarly to CH_4–H_2O mixtures. The modeling results in the present paper explore the differences and similarities between CO_2, H_2O, and air mixtures.

3. Button-cell model

A primary objective of the modeling is to investigate the behavior of species and temperature profiles within the anode structure as functions of fuel composition and barrier-layer design. Details of the button-cell model are documented in previous literature [14–19], so only a brief summary is included here. Gas flows within the fuel and air chambers are modeled as perfectly stirred reactors [17], with fuel utilization depending upon the chamber volume, inlet flow rates, and consumption or depletion via reforming and charge-transfer chemistry.

Electrochemical charge transfer at the anode and cathode interfaces with the dense electrolyte is modeled using a modified Butler–Volmer formulation [14,16]. The effective active area of the triple-phase region is taken as an empirical parameter, which is incorporated into the exchange current density. The model assumes that charge transfer at the anode–electrolyte interface proceeds only through H_2, which is produced as a result of reforming chemistry within the anode structure. Direct charge transfer via CO is

neglected, assuming it to be much slower than the H_2 charge transfer. Because the global water–gas-shift reaction ($CO + H_2O = CO_2 + H_2$) remains nearly equilibrated, much of the CO that is formed via the reforming process is converted to H_2 and CO_2. The resulting H_2 is able to participate in charge transfer.

Reacting porous-media transport within the electrodes is represented using a Dusty-gas model (DGM), which considers pressure-driven convective fluid flow as well as ordinary and Knudsen molecular diffusion. Heterogeneous surface chemistry within the Ni–YSZ anode is represented by a detailed reaction mechanism that incorporates steam and dry reforming as well as partial oxidation [19,20]. This mechanism involves 42 reactions among 6 gas-phase species and 12 surface-adsorbed species. However, the mechanism does not specifically incorporate deposit formation reactions. Because the porous barrier layer is assumed to be chemically inert, only the gas-phase transport is considered within the barrier. Gas-phase chemistry is negligible in the fuel chamber and within the anode pore spaces. The effective thermal conductivity of the solid material within the anode structure was assumed to be 11 W/m K.

In addition to predicting temperature distribution within the anode structure, the model also predicts the membrane–electrode assembly (MEA) temperature relative to the gas and furnace temperatures. Heat is generated within the MEA as the result of ohmic and activation polarizations. Heat is consumed as a result of steam- and dry-reforming chemistry, but heat is produced as a result of partial-oxidation chemistry. The model considers convective and radiative heat exchange between the faces of the MEA and the gas chambers and furnace walls. Depending upon the fuel mixture and the cell operating conditions, the MEA temperature may be above or below the furnace temperature.

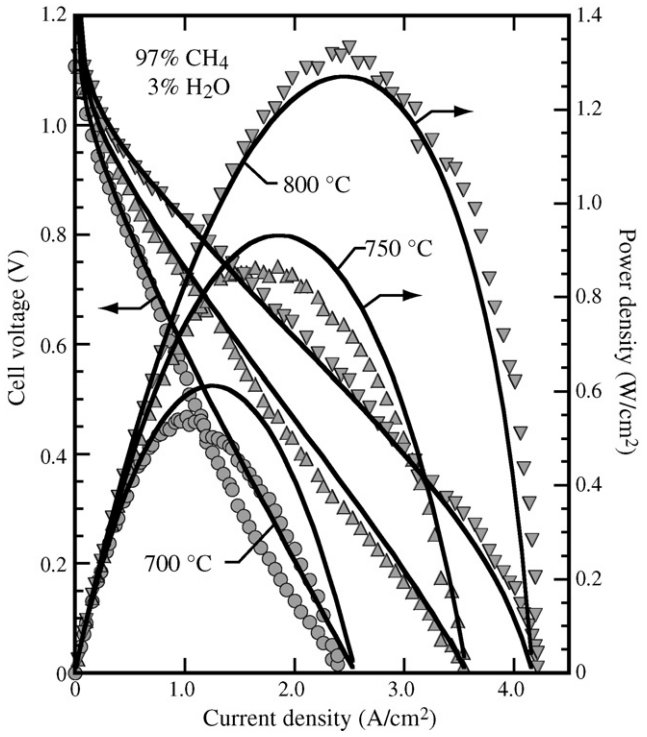

Fig. 2. Measured cell potential and power density as functions of current density for a button-cell MEA structure operating with a fuel mixture of 97% CH_4 and 3% H_2O at 1 atm and temperatures of 700, 750, and 800 °C. The cathode-side oxidizer is air. The solid lines are the model predictions.

4. Experimental results

4.1. Cell electrical characteristics

Figs. 2 and 3 show the polarization performance of two nearly identical button cells (with barrier layers) observed at different temperatures, but with different fuels. In both cases, the anodes were composed of 600 μm of porous Ni–YSZ and 400 μm of a porous barrier layer. The cell represented by Fig. 2 was operated on humidified methane. The cell represented by Fig. 3 was operated on a mixture of 71.4% CH_4 and 28.6% CO_2. The results are typical of anode-supported SOFCs operated with methane, showing relatively high open-circuit voltages and maximum power densities approximately 10% lower than those for hydrogen [3,5]. The addition of 28% CO_2 had little impact on the cell performance—the power density at 800 ° C and 0.7 V was approximately 1.1 W/cm^2 in both cases. At lower temperature, the cell operated on a CH_4–CO_2 mixture showed slightly lower cell resistance, yielding a slightly higher power density (e.g., approximately 0.6 W/cm^2 versus approximately 0.5 W/cm^2 at 700 °C). However, this unexpected result was likely due to variations in cell fabrication.

The model predictions shown in Figs. 2 and 3 depend upon physical parameters, some of which are measured directly (e.g., physical dimensions) and others that must be established empirically (e.g., exchange current densities). The latter parameters were established by achieving a best overall fit to the measured polarization characteristics. Overall, the agreement between the predicted and experimental results was very good. Table 1 lists the physical and model parameters.

Fig. 4 shows measured electrochemical impedance spectra from a cell with a barrier layer operated at 800 ° C under a steady load (current density of $J = 1.6$ A/cm^2) and various CH_4–CO_2 mixtures. The spectra were typical of anode-supported cells operated with

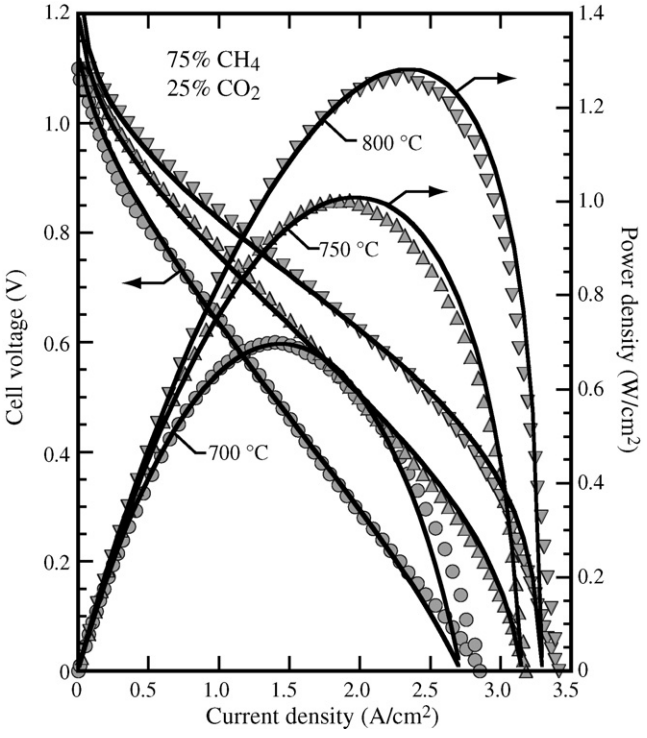

Fig. 3. Measured cell potential and power density as functions of current density for a button-cell MEA structure operating with a fuel mixture of 71.4% CH 4 and 28.6% CO_2 at 1 atm and temperatures of 700, 750, and 800 °C. The cathode-side oxidizer is air. The solid lines are the model predictions.

Table 1
Parameters for modeling the MEA structure.

Parameters	Value
Anode	
Thickness (L_a)	600 μm
Porosity (ϕ)	0.35
Tortuosity (τ)	4.50
Pore radius (r_p)	0.35 μm
Particle diameter (d_p)	1.40 μm
Specific catalyst area (A_s)	1.35E4 cm^{-1}
Exchange current factor ($i^*_{H_2}$)	3.25 A/cm^2
Activation energy (E_{H_2})	85 kJ/mol
Reference temperature (T_{ref})	700 °C
Anodic symmetry factor (α_a)	0.75
Cathodic symmetry factor (α_c)	1.25
Cathode	
Thickness (L_c)	30 μm
Porosity (ϕ)	0.35
Tortuosity (τ)	4.5
Pore radius (r_p)	0.35 μm
Particle diameter (d_p)	1.4 μm
Exchange current factor ($i^*_{O_2}$)	2.00 A/cm^2
Activation energy (E_{O_2})	90 kJ/mol
Reference temperature (T_{ref})	700 °C
Anodic symmetry factor (α_a)	0.5
Cathodic symmetry factor (α_c)	0.5
Electrolyte: $\sigma_{el} = \sigma_0 T^{-1} \exp(-E_{el}/RT)$	
Thickness (L_{el})	13 μm
Activation energy (E_{el})	80 kJ/mol
Ion conductive pre-factor (σ_0)	1.8E5 S/cm
Barrier	
Thickness (L_{el})	400 μm
Porosity (ϕ)	0.4
Tortuosity (τ)	4.00
Pore radius (r_p)	0.40 μm
Particle diameter (d_p)	1.6 μm

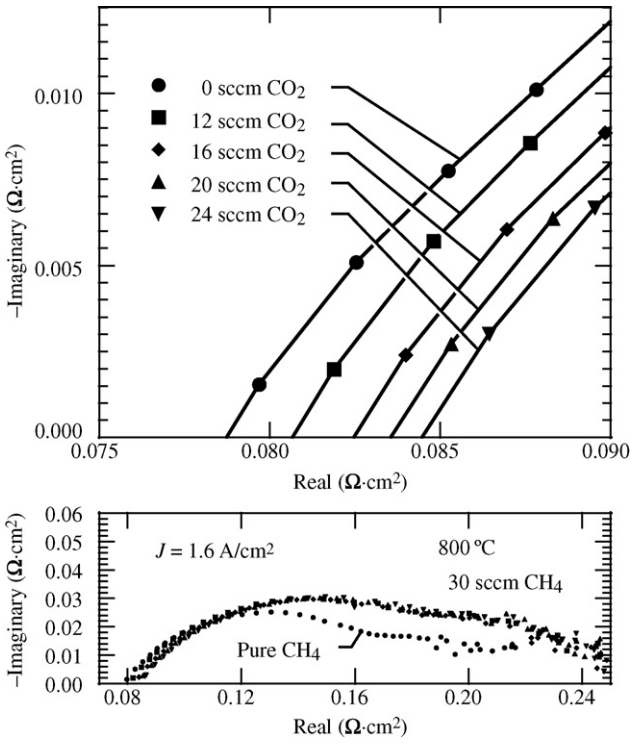

Fig. 4. Electrical impedance measurements at 800 ° C for a cell operating with a range of CH_4–CO_2 fuel mixtures. In all cases, a constant steady current density of 1.6 A/cm^2 was imposed. The shifts in the high-frequency real-axis intercept, though small, were observed reproducibly and in real time as the fuel composition was changed.

methane [3], with a high-frequency intercept on the real axis at approximately 0.08 Ω cm^2 and depressed electrode arcs. The electrode arcs showed only minor changes with fuel composition, in concert with the 800 ° C data in Figs. 2 and 3. The most significant difference was between the pure CH_4 case and the CH_4–CO_2 mixtures, where a significant change in the shape of the arc was observed. There was also a continuous shift of the high-frequency intercept to higher ohmic resistances as the CO_2 content increased (upper panel of Fig. 4). A similar effect was observed previously for internal reforming of iso-octane and was explained by a change in the cell temperature due to the endothermic reforming reaction [21]. The temperature change was estimated from the resistance increase of approximately 8% for the highest CO_2 content, using the temperature-dependent conductivity of YSZ, yielding a temperature reduction of approximately 10 °C.

4.2. Effect of barrier layer

When initial SOFC tests were carried out without barrier layers using fuel mixtures of 75% CH_4 and 25% CO_2, the cells invariably cracked during the first hour of operation. This was tentatively explained as being due to the endothermic catalytic reforming chemistry, which causes local cooling within the anode. The resulting thermal–mechanical stresses presumably caused the cell cracking. However, with a barrier layer in place, the cells did not crack. This result was explained by the fact that the inert barrier layer slowed the reforming rate, thereby reducing the temperature excursion. The cell temperature decrease as estimated via temperature-dependent resistance measured in the EIS experiments was only about 10 °C, which was apparently insufficient to cause cracking. The temperature decrease was probably significantly larger in the non-barrier case, leading to the observed cell cracking. However, the EIS experiments were only possible with the barrier in place to avoid cracking. Cells tested in methane–air mixtures also did not crack, presumably because of small temperature excursions.

It is generally recognized that temperature gradients associated with internal reforming can be the cause of damage in SOFC stacks. One possible approach to moderating temperature gradients in a stack is to vary the catalyst loading spatially, seeking to decrease reforming activity in the stack entry regions. The results here suggest that barrier layers also serve this purpose, as well as limiting deleterious coke formation.

4.3. Baseline results for dry methane

Fig. 5 shows the voltage versus time for a SOFC with barrier measured at 800 ° C in pure CH_4 at different constant current densities. During an initial 10 h test at $J = 1.4$ A/cm^2 the cell voltage was stable. However, when the current density was reduced to

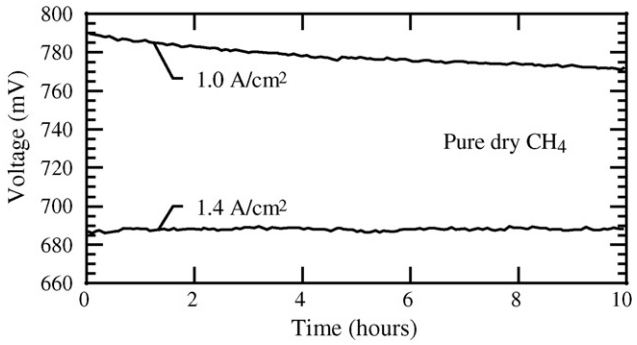

Fig. 5. Voltage versus time for a cell operating on pure dry methane at two current densities.

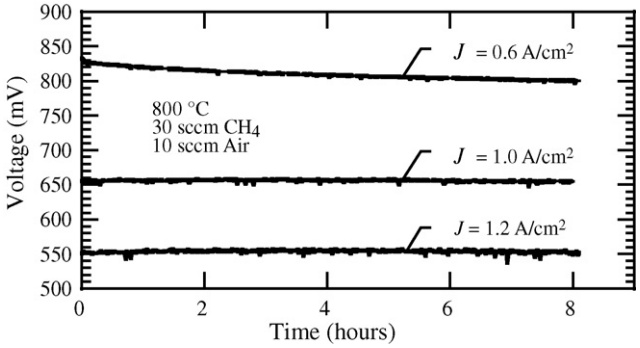

Fig. 6. Voltage versus time for a cell operating on a methane–air mixture at three current densities.

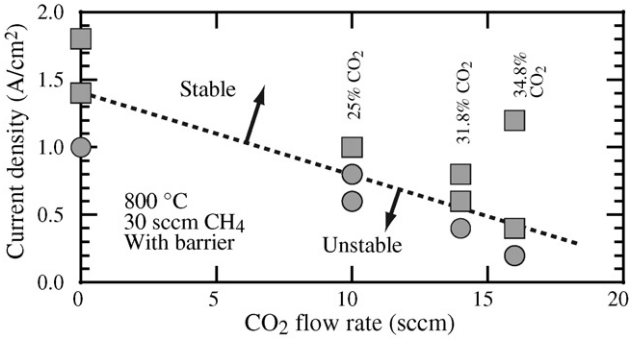

Fig. 8. Map showing whether stable (■) or unstable (•) SOFC operation was observed as a function of CO_2 content and cell current density.

$J = 1.0\,A/cm^2$ the voltage decreased continuously. Post-test SEM-EDS observations revealed anode coking, which coincided with the voltage degradation. This trend, where coking occurred below a critical J value, agrees with prior reports [5]. The critical current value was higher in the present case, probably due to the slightly different nature of the SOFCs and barrier layers used in the present study, and also due to use of dry methane in Fig. 5 compared with humidified methane in the prior work.

4.4. Stability in methane–air mixtures

Fig. 6 shows the voltage versus time for a SOFC operated at 800 °C with a fuel mixture of 75% CH_4 and 25% air. During an initial 8 h test at $J = 1.2\,A/cm^2$, and in a subsequent 8 h test at $J = 1.0\,A/cm^2$, the cell voltage was stable. However, the cell voltage decreased with time at $J = 0.6\,A/cm^2$ due to anode coking. These results indicate that adding 25% air to methane reduced the critical current density for stable operation from $J_c \approx 1.4$ to $1.0\,A/cm^2$.

4.5. Stability in methane–CO_2 mixtures

Fig. 7 a shows voltage histories obtained from a cell that was operated at 800 °C with a fuel mixture of 75% CH_4 and 25% CO_2 (CO_2 flow rate of 10 sccm). At $J = 1\,A/cm^2$ the voltage remained stable for 8 h. At $J = 0.8\,A/cm^2$ the voltage decreased continuously.

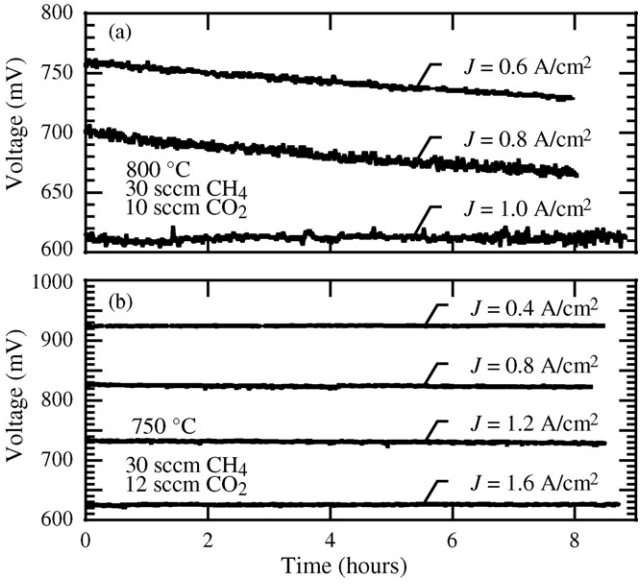

Fig. 7. Voltage versus time for a cell operating on CH_4–CO_2 mixtures at different current densities and temperatures.

Similar degradation was observed at $J = 0.6\,A/cm^2$. These results suggest that the critical current density for stable operation was approximately $1.0\,A/cm^2$. By way of comparison, the same cell and barrier tested with pure CH_4 showed a critical current density of $J_c \approx 1.4\,A/cm^2$.

Fig. 7 b shows the voltage histories for a cell operating with a fuel mixture similar to that in Fig. 7 a, but at a reduced temperature of 750 °C and a higher CO_2 fraction. Under these circumstances the cell voltage remained stable for more than 8 h at each current density, including $J = 0.4\,A/cm^2$. Overall, decreased operating temperature increased the range of current densities for which the operation was stable, which agrees with prior reports [3].

Fig. 8 shows a map of the stable and unstable regimes for SOFCs operated at 800 °C plotted at different CO_2 flow rates and current densities, but with fixed CH_4 flow rate. The dashed line indicates the approximate critical current density J_c required to maintain stable non-coking operation. The critical current density decreased with increasing CO_2 content, with a value as low as $0.4\,A/cm^2$ for 35% CO_2. Note that the dashed line extrapolates to $J_c = 0$ at a CO_2 flow rate of approximately 21 sccm, or approximately 42% CO_2. This value agrees reasonably with the minimum equilibrium non-coking CO_2 content (Fig. 1).

4.6. Effect of CO_2 during current interruptions

The above results pertain to steady-state operation. Given that cell current is required to maintain stable non-coking operation, any interruption of the cell current could potentially cause permanent damage to the SOFC stack. Interruptions may occur during a planned shutdown or as the result of unplanned events. In either case, it is important to know how much time is available before anode coking causes irreversible damage. Depending upon the result, it may be possible to design the SOFC system such that the methane can be flushed from the anode compartment prior to suffering any permanent damage.

Fig. 9 shows the results of current-interruption experiments using two different fuels. Fig. 9 a shows the voltage histories using pure dry methane at $1.8\,A/cm^2$ at 750 °C, with the current reduced to zero for periods of 1.5, 6, and 10 min. For the 1.5 and 6 min interruptions, the voltage immediately after current resumption exceeded the pre-interruption value, and then gradually relaxed to the initial value. This voltage increase was tentatively explained as an effect of carbon deposition on the anode. It was previously suggested that small amounts of carbon deposited during methane operation may increase the cell open circuit voltage [22], which would also increase the voltage while drawing current. The gradual voltage decrease can be explained by removal of the deposited carbon during high-current operation, assuming that the gas composition within the anode is in the non-coking regime. Following a 10 min long interruption, the voltage remained low and

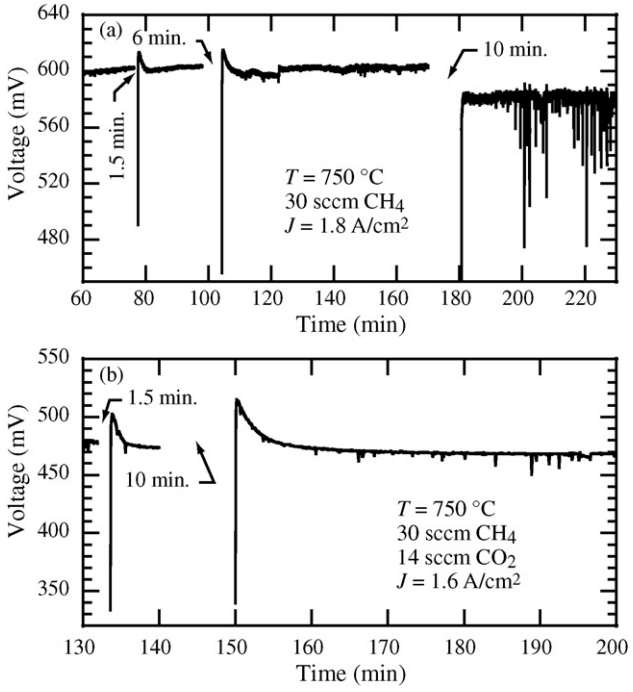

Fig. 9. Current interruption study during SOFC operation at 750 °C. (a) Fuel is CH_4 and (b) fuel is 72% CH_4 and 28% CO_2.

never recovered to its pre-interruption level. This suggests that at longer times, there was sufficient carbon deposition to permanently degrade the cell, perhaps by disrupting the anode microstructure. It was previously shown that carbon deposits can grow sufficiently to fill pores within the Ni–YSZ anode, causing micro-cracking [3].

Fig. 9 b shows voltage histories for a similar cell operated at 1.6 A/cm^2 at 750 °C, but with a fuel mixture of 28% CO_2 and 72% CH_4. After both 1.5 and 10 min interruptions, the voltage relaxed to the steady-state value. In other words, the CO_2 in the fuel mixture enabled a longer interruption without permanent voltage degradation. This result suggests that the CO_2 reduced the rate of anode coking at zero current.

5. Model predictions and discussion

Figs. 10–13 illustrate the effects of the fuel composition and the barrier layer on temperature and species profiles. Four different fuel mixtures were considered: (1) humidified CH_4 (3% H_2O); (2) 75% CH_4 and 25% CO_2; (3) 75% CH_4 and 25% air; and (4) 75% CH_4 and 25% H_2O. In all cases, the inlet CH_4 flow rate was set to be 30 sccm. Temperatures of the external furnace and the inlet fuel stream were fixed at 800 °C. The cells were operated at a current density of 1.5 A/cm^2.

First consider the humidified CH_4 case (Fig. 10). In both the non-barrier and barrier cases, the temperature is considerably below the furnace temperature. This is the result of endothermic steam reforming, with most of the steam being produced by charge-transfer chemistry at the electrolyte interface. Because the current density is the same in both cases, the H_2 flux toward the electrolyte interface is essentially the same. In both cases, there is significant excess reforming in the sense that more H_2 is produced than can be consumed electrochemically at 1.5 A/cm^2. Therefore, the H_2 and CO mole fractions have peak values within the anode structure, with fluxes toward the dense electrolyte and toward the fuel compartment. Because of the excess reforming, significant levels of H_2 and CO are transported into the fuel compartment, rather than being consumed electrochemically.

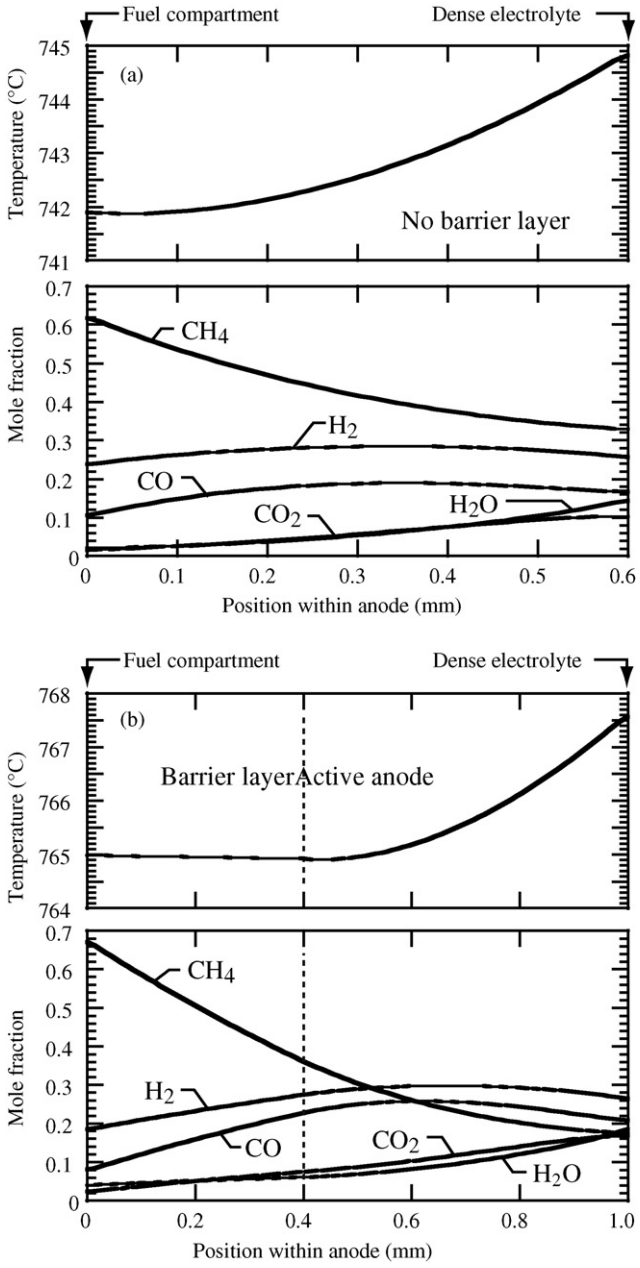

Fig. 10. Calculated temperature and mole-fraction profiles through the anode for a fuel mixture of 97% CH_4 and 3% H_2O with inlet temperature of 800 ° C and pressure of 1 atm. (a) The anode does not include a barrier layer. (b) The anode includes a barrier layer.

Because the barrier layer impedes the transport of CH_4 into, and H_2 out of, the Ni–YSZ anode, the net endothermic reforming rates are lower than they are in the non-barrier case. Evidence for the reduced reforming can be seen by comparing the CH_4 mole fractions at the interface between the anode and fuel compartment (Figs. 10 a and b). The fact that CH_4 level is significantly lower in the non-barrier case means that more methane is converted by reforming. The mole-fraction profiles within the barrier are nearly linear, because surface chemistry does not occur within the barrier.

Because of the increased endothermic reforming in the non-barrier case (Fig. 10a), the temperatures are significantly lower than when the barrier layer is used (Fig. 10b). The temperature profile is nearly flat within the barrier layer because there is no reforming chemistry in that region. As a result of ohmic heating and irreversible processes associated with the charge-transfer chemistry,

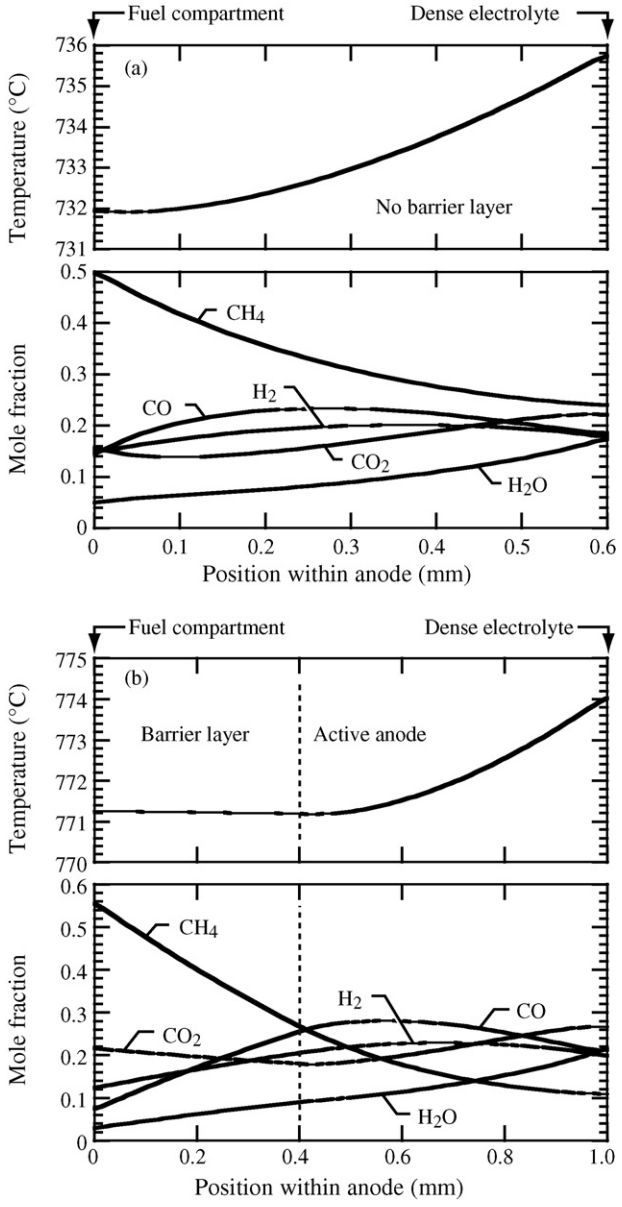

Fig. 11. Calculated temperature and mole-fraction profiles through the anode for a fuel mixture of 75% CH_4 and 25% CO_2 with inlet temperature of 800 ° C and pressure of 1 atm. (a) The anode does not include a barrier layer. (b) The anode includes a barrier layer.

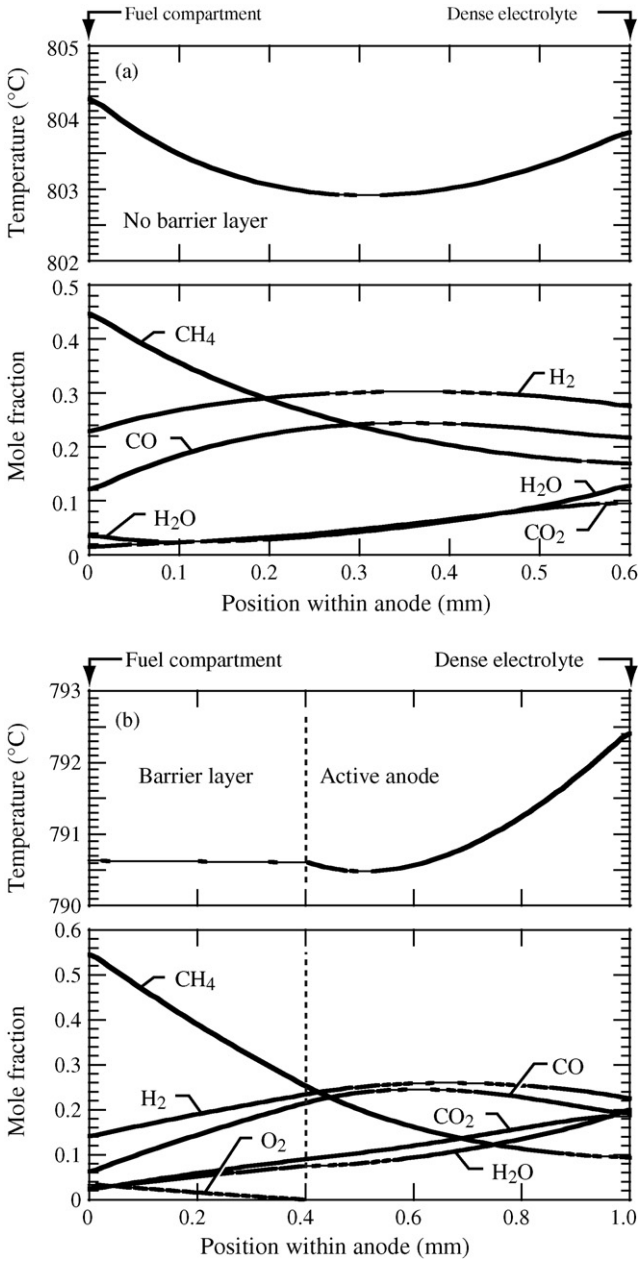

Fig. 12. Calculated temperature and mole-fraction profiles through the anode for a fuel mixture of 75% CH_4 and 25% air with inlet temperature of 800 ° C and pressure of 1 atm. (a) The anode does not include a barrier layer. (b) The anode includes a barrier layer.

the highest local temperatures are near the dense–electrolyte interface, but the net temperature variation through the MEA is only a few degrees. Although the temperature variation within the MEA is generally small, the average temperature of the MEA can vary significantly from the 800 ° C furnace temperature. Indeed, it is this average temperature that is the primary subject of attention here. Thermally induced tensile stresses are introduced when the button cell temperature is significantly lower than that of the surroundings and the supporting ceramic tube. When the temperature reduction is sufficiently large, cracking can occur.

Consider next the cases with a fuel mixture of 75% CH_4 and 25% CO_2 (Fig. 11). As is the situation with humidified CH_4 fuel, the temperatures are lower in the non-barrier cell than they are in the equivalent cell with a barrier layer. In the non-barrier case, the temperatures for the CH_4–CO_2 fuel (Fig. 11a) are lower than they are for the humidified CH_4 fuel (Fig. 10a). The CO_2 from the fuel and the H_2O formed by charge-transfer chemistry both contribute to the endothermic reforming. The result is increased levels of excess reformate (H_2 and CO) and lower temperatures than in the humidified CH_4 case. Because the cells are operated at 1.5 A/cm^2, the H_2 flux toward the dense electrolyte is the same in all cases. Thus, the increased reforming with the CH_4–CO_2 fuel results in more H_2 and CO being transported into the fuel compartment. As in the humidified CH_4 case, H_2 and CO show local maxima within the anode. However, because of excess CO_2 in the fuel and production of CO_2 via water–gas-shift chemistry near the dense electrolyte, there is a local minimum in the CO_2 mole fraction. Also, because of increased carbon in the system, the CO mole fractions is greater than the H_2 mole fractions. This situation is reversed for the humidified CH_4 fuel, where H_2 mole fraction is greater than the CO mole fraction.

It is interesting to note that with the barrier layers operating on CH_4–CO_2 fuel, the average cell temperature is somewhat higher

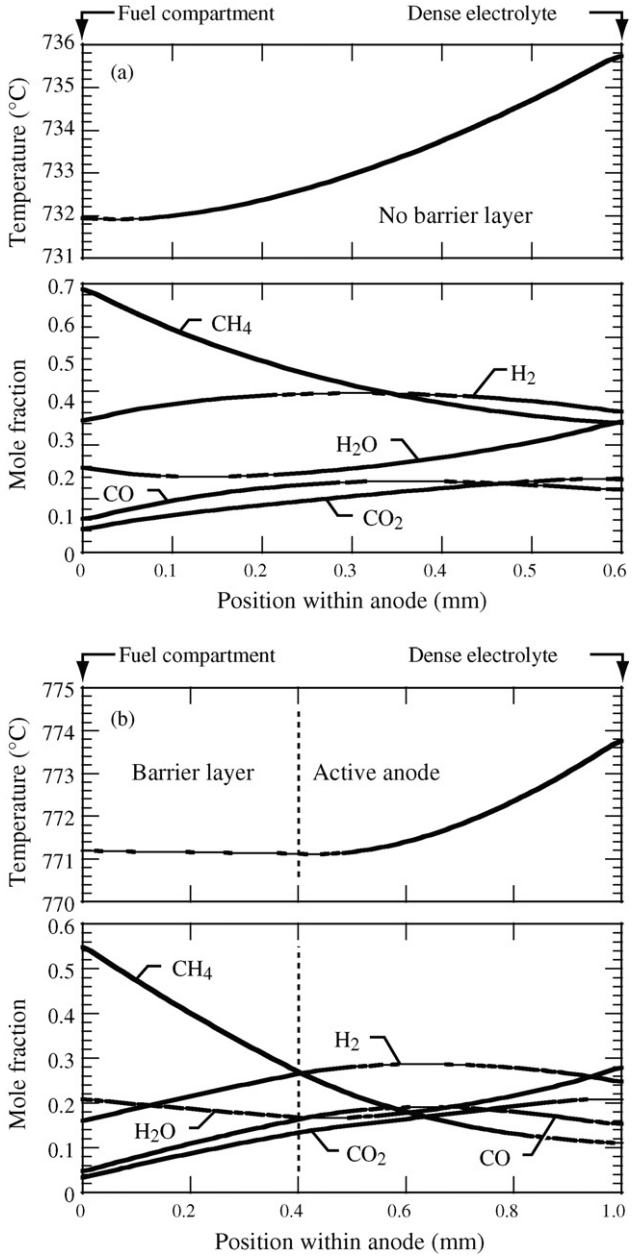

Fig. 13. Calculated temperature and mole-fraction profiles through the anode for a fuel mixture of 75% CH_4 and 25% H_2O with inlet temperature of 800 ° C and pressure of 1 atm. (a) The anode does not include a barrier layer. (b) The anode includes a barrier layer.

(Fig. 11b) than it is for the humidified CH_4 fuel (Fig. 10b). This is opposite the situation for the non-barrier cells. The barrier plays an important role in impeding the transport of CH_4 and CO_2 toward the active part of the anode where Ni catalyzes the reforming chemistry. Because the current density is fixed, the amount of steam available from the charge-transfer chemistry is the same in both cases. In addition to acting as a dry-reforming agent, the excess CO_2 also acts as a diluent with a high heat capacity. The result of these competing factors is that when the barrier is in place the average temperature is lower for the humidified CH_4 fuel than for the CH_4–CO_2 fuel.

The simulation results shown in Figs. 10 b and 11 b can be compared with the experimental cell characteristics shown in Figs. 2 and 3. The simulation shows a temperature that is a few degrees higher for CO_2 case, but a lower H_2 concentration of approximately 20% versus approximately 27% (at the dense–electrolyte interface). These opposing effects suggest that the performance should be similar in the two cases, as is observed. The lower limiting current in the CO_2 case is consistent with the lower H_2 content.

When air is added to the fuel, the temperature behavior changes qualitatively. In the non-barrier case (Fig. 12a), the MEA temperatures are slightly above the furnace temperature. The temperature profile has a local minimum within the MEA. The high temperature at the fuel-chamber interface is the result of rapid exothermic oxidation of the fuel with available air. In fact, the oxidation rate is sufficiently fast that essentially no oxygen survives beyond the surface of the interface between the cell and the fuel chamber. As with the other fuel mixtures, the high temperature at the dense–electrolyte interface is due to the ohmic heating and electrochemical oxidation. With a barrier layer in place, the MEA temperatures are slightly below the furnace temperature (Fig. 12b). Because the barrier impedes the oxygen flux into the chemically active regions of the anode, the exothermic oxidation rate is reduced. At the interface between the barrier and the chemically active portion of the anode, the exothermic oxidation must compete with the endothermic reforming. The slight temperature minimum within the chemically active anode (Figs. 12 a and b) is the result of this competition.

As discussed in Section 4.2, cells without a barrier invariably cracked when operated with CH_4–CO_2 fuel mixtures. This is not surprising in light of the substantial temperature decrease in the button cell that is approximately 65 ° C lower than the environment. The resulting tensile stress produced by differential thermal expansion when the button-cell temperature is lower than that of the supporting tube can cause the cell to crack. As shown in Fig. 11 b, the overall effect of the barrier was to moderate the endothermic reaction rates, thereby decreasing the cell cooling to less than 30 °C, and helping to explain why the cells with a barrier did not crack. Fig. 12 indicates that the temperature deviations in the cells operated with methane–air were much smaller, explaining why the cells without barriers did not crack.

Finally, consider the cases with a fuel mixture of 75% CH_4 and 25% H_2O (Fig. 13). The results are generally similar to those for CH_4–CO_2(Fig. 11). Because the net reforming rates are similar and heats of reaction for dry and steam reforming are similar, the temperature profiles are also similar. As expected, steam reforming leads to higher H_2 and lower CO concentrations than the does dry (i.e., CO_2) reforming, which produces higher CO concentrations relative to H_2.

The predicted effects of the barrier layer and the alternative fuel compositions on anode coking can be assessed in the context of equilibrium coke formation. The coking propensity is greatest at the fuel-compartment side of the Ni-loaded anode structure, where the hydrocarbon (methane) concentration is highest and the concentrations of oxygen-containing compounds are lowest. Based upon predicted compositions (Figs. 10–13), points are plotted on the Gibbs equilibrium triangle (Fig. 1). Without barrier layers, all of the fuel compositions are expected to cause coking (see light-shaded points on Fig. 1). The dark-shaded points on Fig. 1 refer to the composition at the interface between the barrier layer and the Ni–YSZ anode structure. With the barrier, the predicted CH_4–CO_2 and CH_4–H_2O fuel mixtures are close to the coke line at 800 °C, indicating significantly reduced coking propensity. Even with the barrier, the predicted compositions for the humidified CH_4 and the CH_4–air cases lie within the coking region. In all cases, the barrier assists greatly in moving the composition toward the non-coking region. As current density is increased from the nominal 1.5 A/cm^2, the compositions move further toward the equilibrium non-coking regime.

Based upon comparing the modeled cell performance, the equilibrium coke limits, and the experimentally observed performance, it appears that the equilibrium coke limits may be too pessimistic.

That is, coke is not observed under conditions for which equilibrium predicts that coke should be formed. The difference presumably lies in the kinetics. Activation barriers must be overcome to achieve the equilibrium. Nevertheless, the modeling predictions do contribute valuable qualitative insight about barrier design and acceptable operating conditions.

It is interesting to observe that the effect of the barrier is to shift the gas-phase equilibrium composition within the Ni–YSZ structure in the direction of being slightly more carbon rich (Fig. 1). Because oxygen is introduced as a result of the electrochemical charge transfer, it might have been anticipated that the shift would be directly toward the oxygen apex. The shift in the carbon direction may be due to the tendency of the barrier to preferentially trap heavier C-containing molecules within the anode, compared to the relatively facile transport of H_2.

The button-cell results provide interesting and important insights concerning larger cell and stack performance. In a planar channel or tubular fuel cell, axial temperature variations are expected along the length of the channel [23]. Endothermic reforming chemistry tends to lower temperatures near the channel inlet. Assuming high fuel utilization, temperatures are also low near the channel exit because the depleted fuel contributes to lower local current density and thus lower electrochemically produced heat. The result of these competing factors, as well as thermal resistance to the transfer of heat to the exterior environment, often causes peak temperatures in the central regions of the stack. For structural and performance reasons, it is usually desirable to minimize temperature gradients within the stack. Barrier layers can play a potentially important role in moderating stack temperature gradients [7,24].

6. Summary and conclusions

The present experimental results and model-based interpretation have shown that the addition of CO_2 or air to methane improves SOFC stability by suppressing coking in Ni anodes. It was found that barrier layers were necessary for using methane–air and methane–CO_2 mixtures. Without a barrier the cells were often susceptible to cracking, apparently due to thermal–mechanical stresses induced by temperature variations caused by endothermic reforming reactions. Simulation results suggest that the barrier impedes the reforming reactions, thereby reducing temperature excursions. Compared to a conventional anode-supported SOFC operated with methane alone, the combination of a barrier layer together with adding CO_2 or air to methane fuel substantially reduced the critical current density needed for stable operation.

Acknowledgements

The effort at Northwestern University was supported by a grant from Department of Energy HiTEC Program and the American Chemical Society Petroleum Research Fund. The effort at the Colorado School of Mines was supported by a DoD Research Tools Consortium (RTC) program administered by the Office of Naval Research under Grant N00014-05-1-0339.

References

[1] A. Atkinson, S.A. Barnett, R.J. Gorte, J.T.S. Irvine, A.J. McEvoy, M.B. Mogensen, S. Singhal, J. Vohs, Nat. Mater. 3 (2004) 17–27.
[2] S.A. Barnett, Solid oxide fuel cells and systems, in: W. Vielstich, A. Lamm, H. Gasteiger (Eds.), in: Handbook of Fuel Cells, vol. 4, Wiley, Hoboken, NJ, 2003, pp. 1098–1108.
[3] Y. Lin, Z. Zhan, J. Liu, S.A. Barnett, Solid State Ionics 176 (2005) 1827–1835.
[4] K. Sasaki, Y. Teraoka, J. Electrochem. Soc. 150 (2003) A878–A888.
[5] Y. Lin, Z. Zhan, S.A. Barnett, J. Power Sources 158 (2006) 1313–1316.
[6] H. Zhu, A.M. Colclasure, R.J. Kee, Y. Lin, S.A. Barnett, J. Power Sources 161 (2006) 413–419.
[7] H. Zhu, A.M. Colclasure, R.J. Kee, Y. Lin, S.A. Barnett, Tubular solid-oxide fuel cells using either anode recycle or barrier layers, In: U. Bossel (Ed.), Seventh European SOFC Forum, number B0704–060, 2006.
[8] Z. Zhan, Y. Lin, M.R. Pillai, I. Kim, S.A. Barnett, J. Power Sources 161 (2006) 460–465.
[9] M. Dry, Catal. Today 71 (2002) 227–241.
[10] M.R. Pillai, D.M. Bierschenk, S.A. Barnett, Catal. Lett. 121 (2008) 19–23.
[11] J.R. Rostrup-Nielsen, Catal. Today 71 (2002) 243–247.
[12] D.J. Wilhelm, D.R. Simbeck, A.D. Karp, R.L. Dickenson, Process. Technol. 71 (2001) 139–148.
[13] Z. Zhan, S.A. Barnett, J. Power Sources 155 (2006) 353–357.
[14] H. Zhu, R.J. Kee, V.M. Janardhanan, O. Deutschmann, D.G. Goodwin, J. Electrochem. Soc. 152 (2005) A2427–A2440.
[15] H. Zhu, R.J. Kee, J. Electrochem. Soc. 153 (2006) A1765–A1772.
[16] H. Zhu, R.J. Kee, J. Electrochem. Soc. 155 (2008) B715–B729.
[17] H. Zhu, R.J. Kee, J. Power Sources 169 (2007) 315–326.
[18] G. Goldin, H. Zhu, R.J. Kee, D.M. Bierschenk, S.A. Barnett, J. Power Sources 187 (2009) 123–135.
[19] E.S. Hecht, G.K. Gupta, H. Zhu, A.M. Dean, R.J. Kee, L. Maier, O. Deutschmann, Appl. Catal. A 295 (2005) 40–51.
[20] V.M. Janardhanan, O. Deutschmann, J. Power Sources 162 (2006) 1192–1202.
[21] Z. Zhan, S.A. Barnett, J. Power Sources 157 (2006) 422–429.
[22] J. Liu, S.A. Barnett, Solid State Ionics 158 (2003) 11–16.
[23] R.J. Kee, H. Zhu, A.M. Sukeshini, G.S. Jackson, Combust. Sci. Technol. 180 (2008) 1207–1244.
[24] H. Zhu, R.J. Kee, M.R. Pillai, S.A. Barnett, J. Power Sources 183 (2008) 143–150.